NONDESTRUCTIVE MAPPING OF SURFACE FILM PARAMETERS WITH DYNAMIC IMAGING MICROELLIPSOMETRY

Ralph F. Cohn
The Johns Hopkins University Applied Physics Laboratory
Johns Hopkins Road
Laurel, MD 20707

James W. Wagner
The Johns Hopkins University Center for Nondestructive Evaluation
Baltimore, MD 21218

INTRODUCTION

Dynamic Imaging Microellipsometry (DIM) is a rapid, high resolution, full-field imaging ellipsometric technique previously described [1,2]. Development and characterization has advanced through the construction and testing of the semi-automated, second DIM system. Several improvements in the system's design have been implemented, but the basic approach of combining an optical system derived from conventional ellipsometry with video and image processing has been retained. The first DIM system used a Polarizer, Compensator, Specimen, and Analyzer (PCSA) optical system. The current instrument has undergone modification into a Polarizer, Half waveplate, Specimen, Compensator, and Analyzer (PHSCA) configuration. The polarization rotation is now under direct computer control enabling automated operation that greatly facilitates statistical analysis of the instrument's response. Finally, high quality metallic and silicon samples have been studied, refining the previous estimates of the systems accuracy, noise and spatial resolution.

BACKGROUND

Ellipsometry is one of the customary techniques for nondestructively measuring the thicknesses of subwavelength transparent films on polished substrates [3,4]. It is based on the measurement of the relative polarization shift of the light beam after an off-normal angle of incidence reflection from a sample. Software [5] is used to compute film thickness given the complex index of refraction for both the film and the bare substrate, the two ellipsometric parameters Δ and ψ, the wavelength and the angle of incidence. Δ and ψ are derived from the complex reflection coefficients of a surface (the parallel (p) and perpendicular (s) relative to the plane of incidence) which are:

$$r_p = |r_p| \, e^{j\delta_p} \tag{1}$$

$$r_s = |r_s| \, e^{j\delta_s} \tag{2}$$

The phase shift (introduced by the reflection) between the p and s components is labeled Δ. The arctangent of the ratio of the amplitude reflection coefficients is ψ. Thus,

$$\Delta = \delta_p - \delta_s \quad (3)$$

and

$$\psi = \arctan |r_p|/|r_s| \quad . \quad (4)$$

Conventional ellipsometry analyzes the reflected light with a single detector, yielding an average film thickness estimate over a broad surface area [3,4]. When spatially resolved images of film thickness variations are required, the beam is focused to a small spot size and scanned over the surface [6,7,8,9]. This procedure produces very accurate ellipsometric results with good spatial resolution but a poor temporal resolution because scanning requires long data acquisition times. The DIM system and the work of Hurd and Brinker [10] use radiometric detection, creating a novel, much faster approach that can simultaneously utilize multiple detectors forming images, linescans, or arbitrary patterns for specific research goals.

PHSCA System

The first DIM system was based on the standard PCSA ellipsometry system combined with an imaging lens and mosaic focal plane detector [1]. The PCSA layout was nearly identical to that of the current PSCA system (Figure 1), except that the compensator was located between the polarizer and the specimen. A radiometric approach was employed, using the excellent linearity and stability of a Charge Coupled Device (CCD) detector to record the light intensity at 4 analyzer angles. The Δ and ψ maps termed "ellipsograms" were then calculated from the intensity images and known instrument settings. Several problems were encountered. First, the birefringent Glan-Thompson polarizers deviated the optical beam path. In the PCSA system the analyzer rotated and therefore the beam deviation created significant image translations at the CCD camera. Registration was then required to realign the features in the images. This violated the constant system gain assumption because individual photo-detector responses were mismatched, requiring a complex and possibly unstable CCD camera gain calibration to properly compensate the resulting errors.

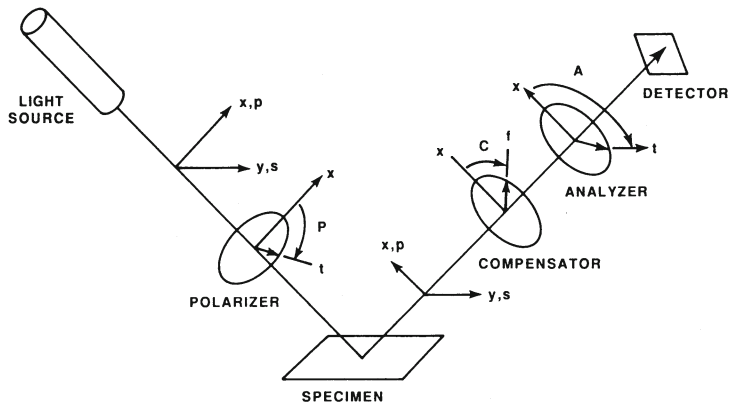

Fig. 1. Optical design of a basic PSCA ellipsometer.

When the component order is rearranged into a PSCA system the polarizer becomes the active optical element and no translation of the specimen image occurs. Therefore, no image registration is needed. The only additional requirement is that the specimen illumination intensity and angle of incidence variations be insignificant compared to other systematic errors, or correctable on a global rather than the local pixel level. For unbiased Δ and ψ measurements, a constant input intensity must be maintained at all polarization angles. This requires that the laser beam be completely circularly or randomly polarized. Any deviations in polarization state introduce systematic error through beam intensity variations which proved to be impossible to eliminate in practice.

A PHSCA optical layout eliminates the beam deviation and intensity variation errors. Both polarizer angles remain fixed and the half waveplate rotates the illumination's linear polarization. The advantages of this approach are threefold. First, the problem of the changing beam path is eliminated since any shifts caused by the half waveplate at normal incidence are insignificant. Second, the beam intensity remains constant within the ability of the CCD camera to measure it (the CCD exhibited a 2% intensity variation relative to polarization, limiting its accuracy). Third, the half waveplate rotates a linear polarization by twice the incoming angle relative to the fast axis. Thus the rotator travels only 1/2 the distance, improving measurement speed. The disadvantage of the PHSCA is that any inaccuracy of the waveplate's retardation adds a new source of systematic error.

To derive the equations for the calculation of Δ and ψ the procedure used in [1] is repeated, changing the component order from PCSA to PSCA. When the Jones vector and matrix computations for light intensity at the detector are repeated for the PSCA system we find that the form of the result remains unchanged with only the P and A angles interchanged. Therefore the PSCA system intensity is:

$$\begin{aligned} I_{PSCA}(P) = {} & (G^2/2)\{[1+\cos 2C \cos 2(A-C)] \cos^2 P \\ & \times \tan^2\psi + [1-\cos 2C \cos 2(A-C)] \sin^2 P \\ & + [\sin 2C \cos 2(A-C) \cos\Delta \\ & - \sin 2(A-C) \sin\Delta] \sin 2P \tan\psi\} \end{aligned} \quad . \qquad (5)$$

with

$$G = K_p K_a K_c |V_{ey}| \quad . \qquad (6)$$

Where the P, C, and A angles are defined in Figure 1 and G represents an overall system gain covering optical component attenuation and the (s) refection amplitude.

Equation 5 has been stated in terms of illumination polarization angle as seen at the specimen which is more intuitively instructive than the half waveplate angle form. When using the half waveplate, an equal polarization rotation is achieved by setting H=P/2 (where H is the half waveplate angle relative to the fast axis).

The approach of using four polarization settings to capture four intensity images is continued. This simplifies the resulting equations and reduces computer calculation time. Images are captured at half waveplate angles of -22.5°, 0°, 22.5°, and 45° which correspond to polarizations of -45°, 0°, 45°, and 90°. Inserting these angles into (5) produces 4 dependent equations that are easily solved with intensities stated in terms of polarization angle producing the following results:

$$\psi = \tan^{-1}\left(\sqrt{\frac{1 - \cos 2C \cos 2(A-C)}{1 + \cos 2C \cos 2(A-C)}}\sqrt{\frac{I(0°)}{I(90°)}}\right) \qquad (7)$$

$$\Delta = \cos^{-1}\left(\frac{I(45°) - I(-45°)}{2\sqrt{I(0°)\ I(90°)}}\right) - \tan^{-1}\left(\frac{\tan 2(A-C)}{\sin 2C}\right) . \qquad (8)$$

The important points observed in equations 7 and 8 remain unchanged from the PCSA case. Neither the input light intensity nor the optical system attenuation are factors in these results. Therefore the system remains free from gain calibration if the system gain G and source intensity are constant during the brief acquisition period for the 4 images. Dark signal offset however must be removed. Also the terms involving the compensator and analyzer angles are separable from the image intensity terms, allowing straightforward correction of azimuth errors via reference sample calibration.

In earlier work [1], the requirement to adjust the PCSA DIM system's optimum measurement range to the specimens ellipsometric parameters was defined to occur when I(A) was constant. The forms of the equations for PCSA and PSCA specifying intensity at the detector are identical. Therefore it follows that the same tuning criteria will produce a constant detector intensity in the PHSCA system. The equations previously developed for determining optimized P and C angles in a PCSA system for a given Δ and ψ pair can be easily adapted by interchanging the P and A angles. Then the two separate equalities which define the optimum A and C angles in the PHSCA system are defined as follows:

$$A = \frac{1}{2} \cos^{-1}\left(\frac{\cos 2\psi}{\cos 2C}\right) + C \qquad (9)$$

and

$$A = -1/2 \tan^{-1}[\sin 2C \tan(\Delta - \pi/2)] + C \quad . \qquad (10)$$

Equations 9 and 10 are then solved simultaneously to determine the optimum A and C angles.

Semiautomatic DIM system

The block diagram in Figure 2 shows the system design of the current PHSCA DIM system. A He/Ne laser at 632.8 nm and a spinning ground glass disk for coherence reduction are used. With the stepping motor rotation

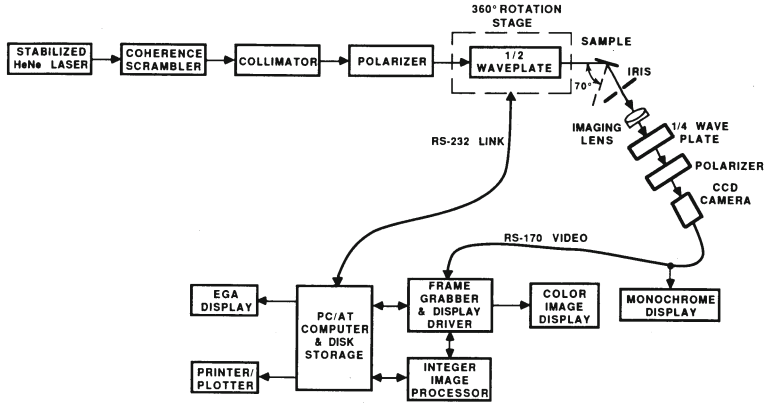

Fig. 2. Block diagram of the full DIM system.

stage under computer control, an automated series of measurements can be programmed. The dark field image is captured at the beginning of the measurement cycle and retained in the image processor allowing immediate correction of each intensity image of the specimen. Repetitive ellipsograms captured from a reference sample are statistically processed to measure random errors and to track temporal drifts in mean Δ and ψ values.

Silicon Wafer Results

DIM System characterization requires stable uniform reference samples with highly polished surfaces. Silicon wafers with silicon dioxide surface films are well suited to these requirements. Two different wafers were studied, an unprocessed polished wafer with approximately a 1.5 to 2.0 nm thick surface film and a processed specimen with a sharp step between two layers with nominal thicknesses of 110 and 55 nm.

Figure 3 shows a surface plot of the four intensity images captured at polarization angles of -45°, 0°, 45°, and 90° with the DIM set in Polarizer, Half waveplate, Specimen, Lens and Analyzer (PHSLA) mode. The analyzer was fixed at A=45°. The images shown in Figure 3 were then processed using equations 7 and 8 to produce the surface map of the ellipsogram shown in Figure 4. The spread that can be observed along the vertical oxide step interface was caused by defocussing resulting from depth of field problems with the sample at a 70° angle of incidence. An improved optical design is being prepared that will increase the depth of field range in the operational DIM system.

Figure 5 shows portions of the theoretical Δ,ψ curves for Si/SiO_2 system at 632.8nm and 69°, 70°, and 71° angles of incidence. The means of the measured Δ,ψ values for the 3 different oxide thicknesses at various analyzer and compensator settings have been plotted. The measured values fall close to the expected theoretical ranges with systematic errors caused by azimuth and alignment errors, waveplate phase delay error, camera/digitizer nonlinearities, and incidence angle error.

The relative spatial accuracy is limited only by the random noise level in the ellipsogram. Tuned system random errors below 0.1° rms for

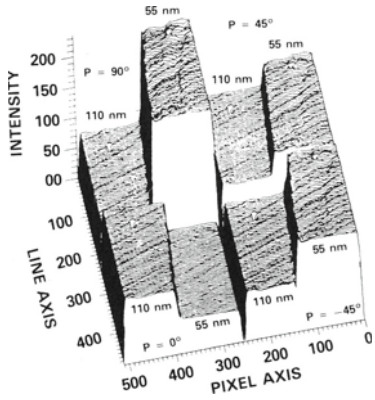

Fig. 3. Intensity surface plots of 55nm/110nm oxide step.

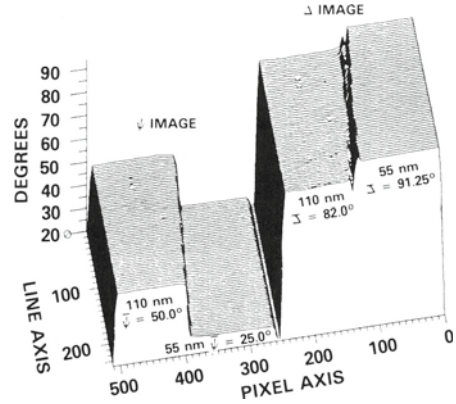

Fig. 4. Ellipsogram derived from data in Fig. 3.

Δ and 0.025° rms for ψ have been demonstrated. These errors yield sufficient relative ellipsometric resolution to permit estimation of thickness variations within oxide layers of intended uniform thickness. Figure 6 shows ψ maps of the 55nm film. This figure is composed of 4

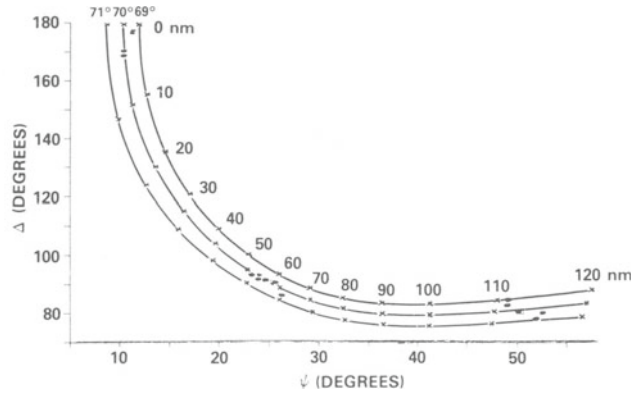

Fig. 5. Theoretical Δ,ψ curves for a SiO_2/Si sample with averaged ellipsogram line values from experiments plotted.

individual measurements each having undergone an XY translation to view a different region of the film. A single blemish remains visible in the central corner of each quadrant image for registration. A hump in the oxide produced a 2° variation in Δ (not shown) and the corresponding inverse 1° variation in ψ is clearly evident. Assuming this is caused purely by a change in the oxide thickness at a constant refractive index, a 3nm or 5% thickness variation is indicated. Thus we have demonstrated that sufficient relative ellipsometric resolution exists for the characterization of thickness variations in "uniform" oxide layers. With improved absolute accuracy through calibration or anticipated design improvements, complete oxide characterization will be possible.

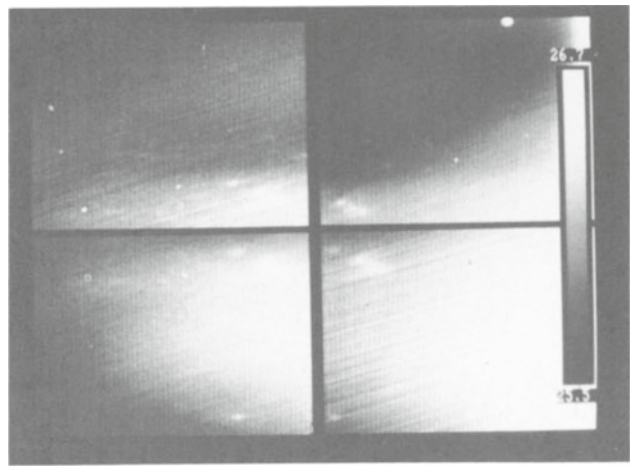

Fig. 6. Four ψ maps of overlapping regions of the 55nm oxide with a common central blemish. Scale units are degrees.

Spatial Resolution

To analyze spatial resolution and further demonstrate inter-frame resolution, measurements were made of metallic samples comprised of niobium wires and fibers in a copper or copper/tin matrix. Three different specimens with feature sizes ranging from 550 to 20 microns were available and the ellipsometric measurements were performed at either high (x15) or medium (x2) magnification as appropriate. Figure 7 shows an ellipsogram at high magnification of 200(v) x 75(h) micron niobium fibers in a copper/tin alloy background. These fibers have been reacted with the matrix forming an outer ring of Nb_3Sn surrounding each fiber. This ring is evident in the ellipsometric results. The affect of defocussing is small and the fibers are clearly observed over the full field of view. Scratches in the surface are also evident, because to maintain a flat surface while polishing the metals of different hardnesses, a short period on a napless wheel was required. This technique does not remove the deeper scratches. The remaining scratches cause scattering and variations in the angle of incidence, which broadens the distribution of ellipsometric values measured. The DIM technique can experimentally observe, separate and quantify the effects of scratches and surface roughness and this is expected to be a significant area for future applications.

Figure 8 shows ellipsometric data from a specimen with 20 to 40 micron diameter unreacted niobium fibers in a copper matrix with a larger tin core visible. The defocussing causes evident errors in this case with the fibers clearly imaged in the approximately 75 image line high central band but largely obscured by defocussing near the top and bottom of the image. Measurements with a 10 micron scale have shown the resolution to be better than 30(v) x 10(h) microns within the focused band. The CCD in a PHSCA system measures a fixed linear polarization, therefore it can be tilted and offset in future systems to better match the focal requirements without causing additional radiometric measurement error.

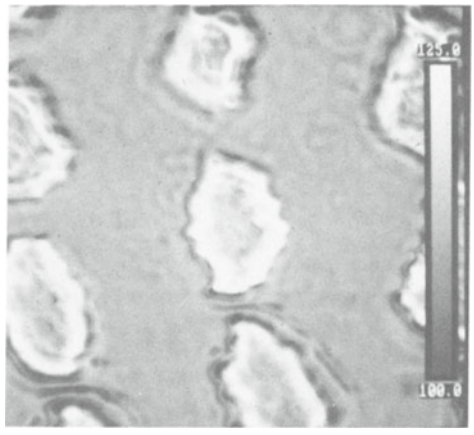

Fig. 7. 200(v) x 75(h) micron Ni fibers in CuSn matrix, Δ map at x15 magnification. Scale in degrees.

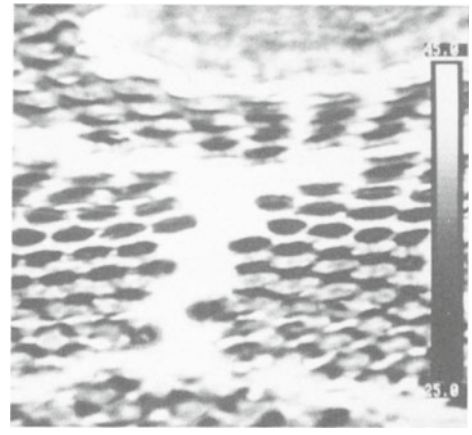

Fig. 8. 20 to 40 micron Ni fibers in Cu matrix with Sn cores, ψ map at x15 magnification. Scale in degrees.

CONCLUSIONS

The Dynamic Imaging Microellipsometry feasibility study has shown that the technique is successful and should prove to be a significant new tool for the evaluation of thin film microstructure. The initial motivation for the DIM feasibility study was to provide a new corrosion research tool for in-situ studies of passive surface film breakdown prior to the initiation of pitting. This goal is near realization and plans to construct a laboratory instrument are underway. Evaluations of DIM's potential applications to other areas of nondestructive testing, such as the measurement of oxide uniformity on semiconductor wafers are also in progress. Sufficient ellipsometric resolution and accuracy have been demonstrated to accomplish the original passive film study objectives and to quickly characterized variations in oxide films. Magnification and depth of field are currently sufficient to measure features on the order of 100 microns across the entire field of view with a spatial resolution better than 10x30 microns at the central focus. Sources of systematic error and defocussing have been identified and will be corrected during the development of the working laboratory DIM system.

ACKNOWLEDGEMENTS

We wish to thank Dr. Norman Blum and Dr. Harry Charles of the JHU/APL Microelectronics Group for providing the Si/SiO_2 step samples. Also Dr. Hugh Issacs of Brookhaven National Laboratory who provided the Cu/Sn/Nb specimens. Support for this work was provided by The Johns Hopkins University Applied Physics Laboratory's Merle A. Tuve Fellowship.

REFERENCES

1. R. F. Cohn, J. W. Wagner and J. Kruger, "Dynamic Imaging Microellipsometry: Theory, System Design, and Feasibility Demonstration", Applied Optics, accepted for pub. June 1988
2. R. F. Cohn, J. W. Wagner and J. Kruger, "Dynamic Imaging Microellipsometry: Proof of Concept Test Results", The Journal of the Electrochemical Society, vol. 135, no. 4, April 1988
3. R. H. Muller, "Principles of Ellipsometry", Advances in Electrochemistry and Electrochemical Engineering, vol.9, Delahay and Tobias, John Wiley and Sons, New York, 1973
4. R. M. N. Azzam and N. M. Bashara, Ellipsometry and Polarized Light, Elsevier Science Publishers B. V., 1987
5. F. L. McCrackin, "A Fortran Program for Analysis of Ellipsometer Measurements", NBS Technical note 479, April 1969
6. K. Sugimoto and S. Matsuda, "Analysis of Passive Films on Austeno-Ferritic Stainless Steel by Microscopic Ellipsometry", Journal of the Electrochemical Society, vol. 130, no. 12, Dec. 1983
7. M. Erman and J. B. Theeten, "Spatially Resolved Ellipsometry", Journal of Applied Physics, vol. 60, no. 3, pp. 859-873, Aug. 1986
8. D. J. Dunlavy, R. B. Hammond and R. K. Ahrenkiel, "Scanning Microellipsometer for the Spatial Characterization of Thin Films", Los Alamos National Labs Report LA-UR-81-1806, 6p, 1981
9. "Auto Gain Ellipsometers", Bulletin EE, p. 13, Gaertner Scientific Corp.
10. A. J. Hurd and C. J. Brinker, "Ellipsometric Imaging of Drying Sol-Gel Films", Better Ceramics through Chemistry III, MRS, 1988